C. R. Mecanique 339 (2011) 466–472

Contents lists available at ScienceDirect

Comptes Rendus Mecanique

www.sciencedirect.com

Surface mechanics: facts and numerical models

# Contact response of ceramics

Eric Le Bourhis

*Institut Pprime, département PMM, UPR 3346 CNRS, Université de Poitiers, ENSMA, SP2MI-Téléport 2, boulevard Marie et Pierre Curie, B.P. 30179, 86962 Futuroscope-Chasseneuil cedex, France*

ARTICLE INFO

*Article history:*
Available online 21 June 2011

*Keywords:*
Contact
Ceramics
Coating
Elasticity
Plasticity
Fracture

ABSTRACT

Instrumented indentation mechanics and its applications to ceramics characterisation are described and discussed. Instrumented nanoindentation has become an outstanding tool for characterising surfaces and is routinely used in industry and university. The article reviews important procedures and concepts that have proved to be very useful to analyse the contact response of ceramics (elastic–plastic loading, indentation strains and stresses, crack generation, composite response of coated pieces). Examples are used to illustrate the very wide range of studies that can be carried out.



## 1. Introduction

Failure in brittle ceramics originates from a defect generally at the surface of the specimen. Fracture starts at a critical defect or flaw and further propagates. The flaw at the origin of fracture can be easily detected in ceramics where, among the broken pieces, is detected a smooth mirror zone at the centre of which the flaw is localised [1]. The way superficial flaws are generated is complex, happening at points of contact with the presence of high stress and strain concentrations and gradients. In the literature, two schematic contact conditions are generally considered. Blunt contact conditions consider that the material under a sphere deforms elastically up to brittle fracture (supposing the surface is damaged, otherwise, presumably the yield stress is less than the flaw-free strength). In contrast, under a sharp contact (addressed here) the material deforms elastically, plastically and finally fractures. The way plastic deformation extends on increasing applied load is extensively discussed and modelled. Both plastic zone and fracture developments after full unloading are then discussed. Moreover, industry has a strong interest in developing new functional coatings. The mechanical performance is then of primary importance to keep this functionality over time. The mechanical performance comprises the properties of the films, the interface and the substrate. The range of thickness for coating is very broad going from several nanometres to several microns where so-called instrumented indentation techniques allow monitoring the mechanical response as a function of the relative penetration and extract relevant properties.

## 2. Instrumented indentation technique

Instrumented indentation allows monitoring the penetration of a tip as a function of load [2,3]. Sharp ones (addressed here) are generally three-faced Berkovich tip allowing for a better definition of the contact area $A_c$ as compared to a Vickers four-faced one. However, the aspect ratio is the same for both tips: $A_c = 24.5h_c^2$, where $h_c$ is the contact depth. The extraction of mechanical properties has focused on the unloading curve employing the well known 'Oliver and Pharr' method [3]. One major assumption of this method is that only elastic recovery happens while unloading, which might not be strictly the case when films show viscoelastic response [1]. Secondly, the methodology was derived from solution of

*E-mail address:* eric.le.bourhis@univ-poitiers.fr.

1631-0721/$ – see front matter 
doi:10.1016/j.crme.2011.05.005

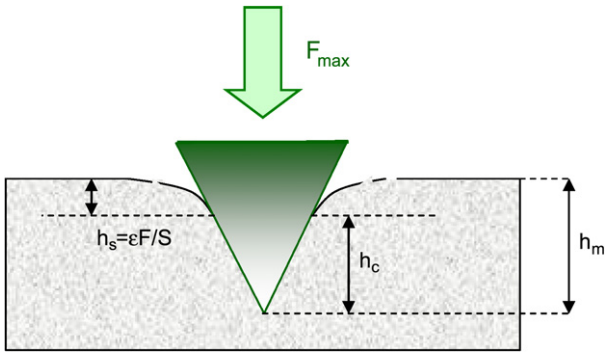


**Fig. 1.** Indentation profile schematics.

elastic contact problems while prior to unloading the contact conditions involve plastic deformation. Thirdly, the material around the contact may exhibit substantial pile-up or sink-in, the projected contact area being then either underestimated or overestimated with errors on the hardness and modulus values.

An important parameter is the contact stiffness ($S = \mathrm{d}F/\mathrm{d}h$) or say the slope at maximum load $F_m$ of the unloading curve that can be fitted by [3]:

$$F = k(h - h_r)^m \quad 1 < m < 2 \tag{1}$$

where $F$ is the load applied to the indenter, $h$ its penetration, $h_r$ the residual depth (after complete unloading). $S$ is then determined to be

$$S = km(h_m - h_r)^{m-1} \tag{2}$$

where $h_m$ is the maximum penetration of the indenter. The contact depth $h_c$ (Fig. 1) is then given by

$$h_c = h_m - \varepsilon F_m/S \tag{3}$$

$\varepsilon$ is about 0.75 and slightly changes with m. Then, hardness $H$ is calculated as the mean pressure over the contact area

$$H = F_m/A_c \tag{4}$$

It should be noted that hardness values obtained from instrumented nanoindentation and microindentation may differ significantly and this phenomenon is invoked as indentation size effect (ISE). Instrumented nanoindentation allows one to further extract the composite indentation elastic modulus (specimen-tip) $E^*$ as:

$$E^* = \frac{S}{2\beta}\sqrt{\frac{\pi}{A_c}} \tag{5}$$

$\beta$ is a correcting factor depending on the tip geometry ($\beta = 1.034$ for a Berkovich one) and $E^*$ is taken as:

$$\frac{1}{E^*} = \frac{1-\nu_D^2}{E_D} + \frac{1-\nu_S^2}{E_S} \tag{6}$$

where $E$ and $\nu$ are the Young modulus and Poisson ratio, subscripts $D$ and $S$ are for diamond and specimen respectively ($E_D = 1141$ GPa, $\nu_D = 0.07$). The reduced modulus is often referred as

$$\frac{1}{E_r} = \frac{1-\nu_S^2}{E_S} \tag{7}$$

As stated above, one major assumption is that unloading is purely elastic. Hence, time dependent material response is to be controlled carefully [1]. Dramatic effects are expected when testing times scale with the characteristic relaxation time of the material: $T_R = \eta/G$ with $\eta$ and $G$ the viscosity and shear modulus of the tested material respectively.

## 3. Indentation strain and stress

Conical indentation generates above a given threshold a plastic zone surrounded by the undeformed solid. Hence, a plastic-strain gradient remains after unloading the specimens. The representative indentation strain $\varepsilon_R$ was defined as [4,5]:

$$\varepsilon_R = 0.2 \operatorname{tg} \beta \tag{8}$$

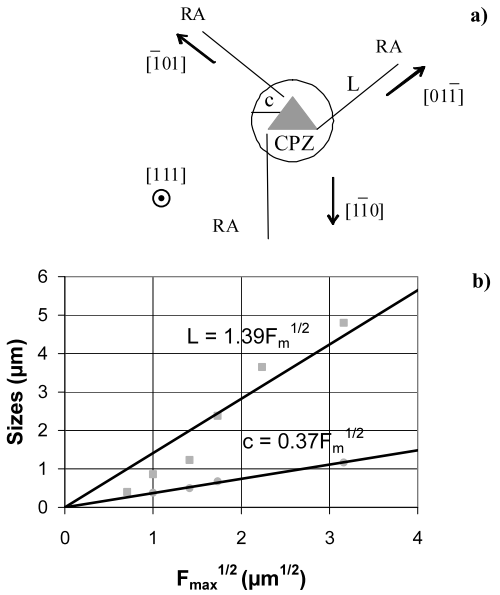


**Fig. 2.** (a) Schematic representation of the indentation plastic zone composed of a central and dense plastic zone (CPZ, radius $c$) and rosette arms extending further out (RA, 3 being shown with length $L$). (b) Central plastic zone radius c and length $L$ of the rosette arms as a function of the square root of the maximum applied load ($\sqrt{F}_{\max}$) at the (111) indented surface of GaAs crystal [12].

where $\beta$ is the angle between the original surface and the conical indenter flank. Under a conical indenter the representative strain remains unchanged (assuming a perfect sharpness of the tip), property that is often referred as self-similarity (refer also to the Alcala and Esqué-de los Ojos article in this issue). This property is to be attributed to the geometric similarity of the tip ($A_c \propto h_c^2$ where $h_c$ is the contact depth). The actual strain values in the vicinity of the tip extremity (∼20–30%) are considerably higher than the representative strain $\varepsilon_R$ value (about 7.2% Eq. (8) with $\beta = 19°$ for a Berkovich or a Vickers tip) that is to be considered as an averaged strain [6,7].

Hardness is generally assumed to be proportional to the representative flow stress $Y_R$ measured in simple compression at the representative strain $\varepsilon_R$ [4,5]:

$$H = CY_R = CY(\varepsilon_R) \tag{9}$$

Considering the equilibrium under load $F$, and balancing the radial forces at the elastic–plastic boundary allows one to obtain the central and dense plastic zone radius $c$ as [8]:

$$c = \sqrt{\frac{3}{2\pi}\frac{1}{Y_R}}\sqrt{F} \tag{10}$$

On the other hand, the rosette arm (RA) expansion after full unloading is driven by the residual stresses generated by the central and highly strained volume, its length $L$ being given by [9,10]:

$$L = \frac{\chi^{1/4}}{\psi^{1/2}}\frac{1}{\tau_c^{3/4}}\sqrt{F_m} \tag{11}$$

with $F_m$ the maximum load that was applied to the indenter (we consider here the unloaded state), $\tau_c$ the critical shear stress of the crystal, $\psi$ a constant about 6, and $\chi$ being obtained from the elastic constants of the crystal

$$\chi = 0.156E(1-\nu) \tag{12}$$

Interestingly, latter model can be extended to thermal relaxation of indents during a post-annealing procedure [11].

Fig. 2 plots the central plastic-zone size $c$ as well as the rosette arm length $L$ as a function of the square root of the maximum load $\sqrt{F}_{\max}$ measured in an indented single crystal ((111) GaAs [12], measured on transmission electron microscopy (TEM) plan views). Both $c$ and $L$ were found to increase linearly with $\sqrt{F}_{\max}$ as expected from Eqs. (10) and (11) (more discrepancies being obtained for $L$, however).

The slopes of the linear fits allow for determining a flow stress about 3.5 GPa with $H/Y_R$ ratio to be about 2.6 close to the value expected from the expanding cavity model ($H/Y_R \sim 3$) [5,12] and a critical shear stress value at about $\tau_c = 0.5$ GPa slightly lower than that obtained on a (001) oriented surface with observed differences in the plastic flow (from three-fold to two-fold symmetry [10,12]).

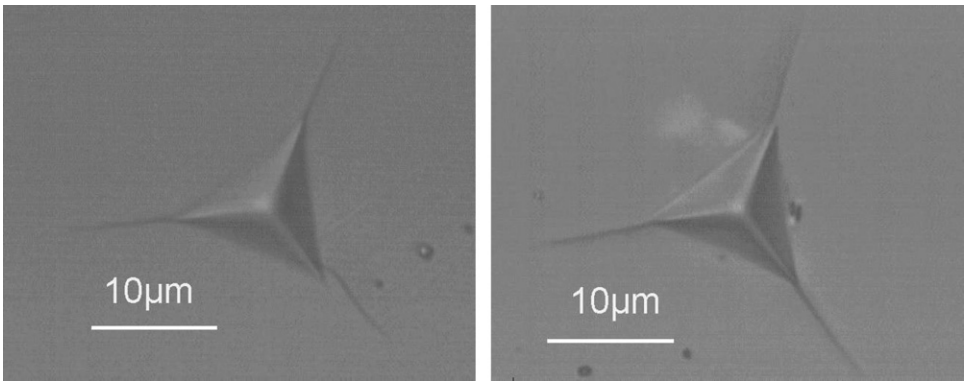


**Fig. 3.** Berkovich indentation test at room temperature on the precursor glass ($50GeO_2$, 42PbO, $8PbF_2$, $3ErF_3$, left) and its vitroceramics (right).

**Table 1**
Summary of the glass and glass ceramics responses under a Berkovich indenter. The precursor glass composition is $50GeO_2$, 42PbO, $8PbF_2$, $3ErF_3$, later annealed at 386 °C for 10 h to form the glass ceramics. $N_{100}$ and $N_{300}$ are the average numbers (± SD) of observed cracks at 13 different indents under 100 and 300 mN respectively. $H$, $E_r$, $K_c$ and $B$ are the determined hardness, reduced modulus, indentation toughness and brittleness index respectively.

| | G31 | G31Vitro |
|---|---|---|
| $N_{100}$ (100 mN) | $1.0 \pm 0.9$ | $1.3 \pm 1.1$ |
| $N_{300}$ (300 mN) | $2.5 \pm 0.7$ | 3.0 |
| $H$ (GPa) | $4.15 \pm 0.05$ | $4.30 \pm 0.06$ |
| $E_r$ (GPa) | $56.08 \pm 0.47$ | $60.0 \pm 0.85$ |
| $K_c$ (MPa $m^{1/2}$) | $0.33 \pm 0.05$ | $0.27 \pm 0.04$ |
| $B = H/K_c$ ($\times 10^3$ $m^{-1/2}$) | $12.6 \pm 2.1$ | $15.9 \pm 2.6$ |

## 4. Elastic–plastic–brittle response

On increasing progressively the applied load, elastic–plastic deformation changes into elastic–plastic–brittle with radial cracks appearing [1] as in a $GeO_2$–PbO based glass developed for optical applications (Fig. 3). This precursor glass was later heat-treated at 386 °C for 10 h to obtain a glass ceramics with a homogeneously distributed crystalline phase (17 nm average crystallite size [13]). The number of observed cracks was observed to increase progressively from 0 under 30 mN (no cracks below this threshold load) to 3 under 300 mN in the case of the glass ceramics as shown in Table 1. Crack threshold is quite sensitive to the experimental conditions with large variations reported between authors [14]. Here, we focus on the comparison between two systems behaviours (precursor glass and glass ceramics) obtained under the same conditions (e.g. atmosphere, loading-unloading and observation sequence). Fig. 3 shows micrographs of both the glass and glass ceramics surfaces after indentation at room temperature (RT) under 300 mN, cracks appearing from the corners and developing almost in straight line.

The extension of the radial cracks is related to the apparent indentation fracture toughness $K_c$ of the glass as proposed originally by Antis et al. [15]. The relation between $K_c$ and the mean size of the cracks $c$ is given by

$$K_c = \chi_r \frac{F_m}{c^{3/2}} \tag{13}$$

where $F_m$ is the load applied on the indenter and $\chi_r$ is a function of the elastic–plastic ratio $E/H$ that informs on the intensity of indentation residual stress field (induced by the 'plastic' zone, proportional to $\chi_r F_m$) yielding crack propagation (for a Berkovich or Vickers indenter $\chi_r = 0.016\sqrt{\frac{E}{H}}$).

Having determined $H$ and $E$ from uncracked indents (force of 30 mN, supposing $\nu = 0.2$) the toughness values reported in Table 1 could be obtained. It is to be noted that the ceramisation hardened the material while it made it more brittle. Noticeably, Eq. (13) is valid for fully developed cracks and in the absence of residual stresses. First requirement would be better fulfilled using a cube-corner tip [16] while an annealing of 2 h at 300 °C that is below $T_g$ (about 350 °C) and below the crystallisation temperature (386 °C) was carried out to reduce stresses [12], the threshold load for cracking being shifted to higher values in the presence of compressive stresses otherwise [1]. The toughness value of PbO–$GeO_2$ is expected to diminish as PbO is introduced to $GeO_2$, assuming a similarity with the $SiO_2$–PbO system [17] while $GeO_2$ toughness value is expected at about 0.6 MPa $m^{1/2}$ lower than that of $SiO_2$ about 0.8 MPa $m^{1/2}$ [18]. Hence, the obtained toughness values are not unexpected for the studied complex glass with main components being $GeO_2$–PbO. The threshold load necessary to pop-in a crack is considered to be an increasing function of $K_c B^{-3}$ [1]. Using similar loading conditions a soda-lime-silica (SLS) glass resisted cracking while its toughness and brittleness index are about 0.7 MPa $m^{1/2}$ and 8.2 $\mu m^{-1/2}$. Hence, SLS

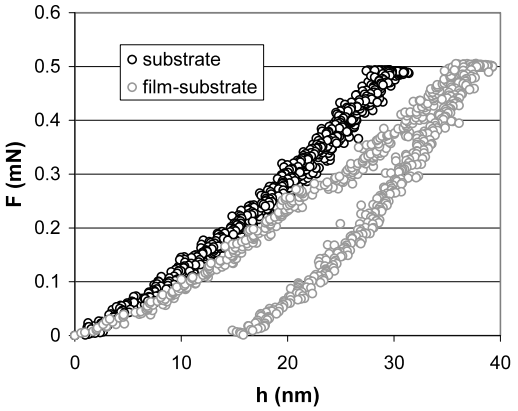


**Fig. 4.** Loading unloading curves obtained for bulk and Au-coated GaAs, under a maximum load 0.5 mN. A slight pop-in excursion is observed under a load of 0.3 mN in the film–substrate specimen [19].

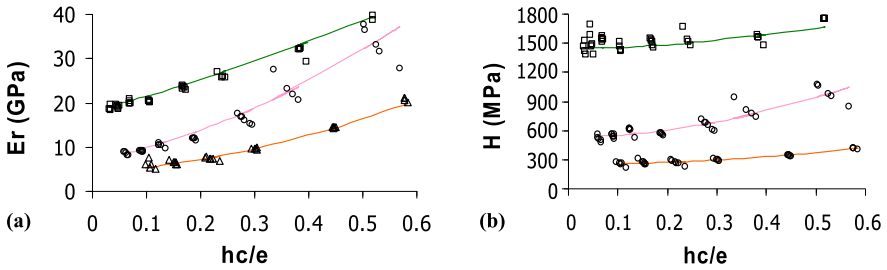


**Fig. 5.** (a) Indentation modulus $E_r$ and (b) hardness $H$ as a function of indentation depth scaled with the coating thickness ($h_c/e$) for (□) pure sol-gel silica (PMMA0), (○) PMMA50 and (△) PMMA100. The adjusted curves are shown as continuous lines [28]. The numbers shown after PMMA corresponds to PMMA wt%.

resistance is expected to be higher than the glass and glass-ceramics studied here in good agreement with the observed behaviours (Table 1).

## 5. Coated-substrate response

The presence of a coating changes dramatically the response of a surface as illustrated in Fig. 4 for GaAs coated with an Au film as thin as 8.9 nm. With the presence of the film, plastic deformation is detected for loads as low as 0.2 mN, while a bare substrate remains elastic. When coated, the plastic onset of the ceramic substrate is modified as well probably because of the change in stress distribution and interface modification during the deposition process [19]. Here, the slight pop-in event is assumed to be related to the substrate. Such events are commonly observed (discontinuity in the loading curve) and believed to be associated to the poor initial defect density. On a coated substrate, this event is less obvious but detected just below 0.3 mN while it is observed above 0.5 mN in the bare substrate [19].

For thicker films, Mencik et al. [20] reviewed models to predict the indentation modulus of homogeneous thin films of thickness e deposited onto a substrate (also supposed to be homogeneous). All of them compose the substrate and film properties:

$$\frac{1}{E_r} = \frac{1}{E_r^s}\phi\left(\frac{h_c}{e}\right) + \frac{1}{E_r^f}\left(1 - \phi\left(\frac{h_c}{e}\right)\right) \tag{14}$$

where $s$ and $f$ superscripts are for the substrate or the film respectively. $E_r$ denotes the measured substrate–film composite property. Assuming a given function $\phi$, allows determining the unknowns ($E_r^f$) once $E_r^s$ is characterised and $E_r$ measured as a function of contact penetration $h_c$. This is illustrated below. It is to be emphasised that the precise form of function $\phi$ as well as its combination with properties (moduli, reduced moduli, inverse of moduli) is still the subject of ongoing researches which employ both analytical as well as numerical approaches [21–24].

A similar procedure can be applied to determine the hardness of the films as reviewed by Beegan and Laugier [25]. Noticeably, at equal indentation depth, the influence of the substrate on the measured hardness is lower than on the indentation modulus since the plastic strain field is much less extended spatially than the elastic strain field. The exponential law proposed by Bhattacharya and Nix is often used [26]:

**Table 2**
Mechanical characteristics of PMMA-$SiO_2$ hybrid materials. The numbers shown after PMMA corresponds to PMMA wt%.

| Specimen | $E$ (GPa) | $H$ (GPa) | $H^3/E^2$ (MPa) |
|---|---|---|---|
| PMMA100 | 4.1 | 0.25 | 1 |
| PMMA75 | 7.6 | 0.49 | 2 |
| PMMA50 | 6.6 | 0.53 | 4 |
| PMMA25 | 9.5 | 0.84 | 7 |
| Sol-gel silica (PMMA0) | 17.5 | 1.48 | 11 |

$$H^* = H_s + (H_f - H_s) \cdot \exp\left[-\alpha \cdot \left(\frac{h_c}{e}\right)^n\right] \tag{15}$$

where $s$ and $f$ subscripts are for the substrate or the film respectively. $H^*$ denotes the measured substrate–film composite property. For soft coatings on hard substrates, $n = 2$ ($n = 1$ on the contrary).

We applied this approach to glass pieces coated by PMMA-$SiO_2$ organic–inorganic hybrids after consideration of their time dependence properties ([27] see Section 2). The increase in the mechanical properties as the indentation depth increases results from the strong influence of the substrate (Fig. 5). It is to be noted that sol-gel silica is less polymerised than fused silica. Hence, a film formed by pure sol-gel silica still shows an increase in both modulus and hardness as relative penetration increases. The indentation modulus adjustment was made using $\phi = 1 - \exp(-\beta \cdot \frac{h_c}{e})$, the determination of the unknowns $(E_f, \beta)$ being made by subtracting $1/E_s$ to $1/E^*$ and applying the least-square method to the logarithms [28]. $H_f$ and $\alpha$ as well could be determined using a least-square method to the logarithms of hardness numbers. Of course, these equations do not take the influence of fracture into account. However, PMMA-$SiO_2$ hybrid materials may present this kind of mechanical behaviour above large critical loads, beyond the range used here to extract the film properties [28]. Consequently, models encompassing elasticity and plasticity can be applied, the extracted results being shown in Table 2. The trends are found in good agreement with layers composition since an improvement of both indentation modulus and hardness versus the silica content was observed. Important also is the increase of $H^3/E_r^2$ ratio which can be used to predict the tribological performance [1], a range of one magnitude being obtained.

Further insights into the mechanical behaviour of composites and thin films can be gained scrutinising the interfaces [29] and the distribution of the reinforcing phases [30].

## 6. Conclusion

Instrumented indentation has been widely used for characterising elastic–plastic–brittle response of ceramics. It is routinely employed in industry and university allowing for determining the mechanical performance of both bare and coated pieces, latter response being of primary importance for keeping new surface functionality in time. Indentation mechanics has been much explored and allows for great insight into the contact response. However, indentation strain and stress gradients are to be considered carefully both during loading and unloading. As regard coated ceramics, films are generally considered homogeneous (no composition-structure gradient) while an important literature still debates on the form of substrate–film properties combinations which allow extracting the composite response.

## Acknowledgements

The author would like to thank Dr. G. Patriarche, Dr. F. Mammeri, Dr. L. Rozes, Dr. C. Sanchez, Dr. D. Faurie, Dr. P.O. Renault, Dr. P. Goudeau, Dr. G. Dantelle, Dr. M. Mortier for collaboration.

## References

[1] E. Le Bourhis, Glass Mechanics and Technology, Wiley–VCH, Germany, 2008.
[2] J.L. Loubet, J.M. Georges, O. Marchesini, G. Meille, Vickers indentation curves of magnesium oxide (MgO), J. Tribology 106 (1984) 43–48.
[3] W.C. Oliver, G.M. Pharr, An improved technique for determining hardness and elastic modulus using load and displacement sensing indentation experiments, J. Mater. Res. 7 (1992) 1564–1583.
[4] D. Tabor, Hardness of Metals, Oxford University Press, 1951.
[5] K.L. Johnson, Contact Mechanics, Cambridge University Press, 1985.
[6] M.M. Chaudhri, Subsurface strain distribution around Vickers hardness indentations in annealed polycrystalline copper, Acta Mater. 46 (1998) 3047–3056.
[7] L. Largeau, G. Patriarche, E. Le Bourhis, Subsurface deformations induced by a Vickers indenter in GaAs/AlGaAs superlattice, J. Mater. Sci. Lett. 21 (2002) 401–404.
[8] D. Kramer, H. Huang, M. Kriese, J. Robach, J. Nelson, A. Wright, D. Bahr, W.W. Gerberich, Yield strength predictions from the plastic zone around nanocontacts, Acta Mater. 47 (1999) 333–343.
[9] M.M. Chaudhri, Dislocations in solids, Ed. F.R.N. Nabarro Collection 2004, Chapter 70.
[10] E. Le Bourhis, G. Patriarche, Structure of nanoindentations in n and p heavily doped (001)GaAs, Acta Mater. 56 (2008) 1417–1426.
[11] E. Le Bourhis, G. Patriarche, Structure of annealed GaAs(001) nanoindentations, J. Appl. Phys. 106 (2009) 123516.
[12] E. Le Bourhis, G. Patriarche, L. Largeau, J.P. Rivière, Polarity-induced changes in the nanoindentation response of GaAs, J. Mater. Res. 19 (2004) 131–136.
[13] G. Dantelle, M. Mortier, D. Vivien, G. Patriarche, Nucleation efficiency of erbium and ytterbium fluorides in transparent oxyfluoride glass-ceramics, J. Mater. Res. 20 (2005) 472–481.

[14] A. Mikowski, F.C. Serbena, C.E. Foerster, C.M. Lepienski, Statistical analysis of threshold load for radial crack nucleation by Vickers indentation in commercial soda-lime silica glass, J. Non-Crystal. Sol. 352 (2006) 3544–3549.
[15] G.R. Anstis, P. Chantikul, B.R. Lawn, D.B. Marshall, A critical evaluation of indentation techniques for measuring fracture toughness: I. Direct crack measurements, J. Am. Ceram. Soc. 64 (1981) 533–538.
[16] G.M. Pharr, Measurement of mechanical properties by ultra-low load indentation, Mater. Sci. Eng. A 253 (1998) 151–159.
[17] E. Vernaz, L. Larche, J. Zarzycki, Fracture toughness-composition relationship in some binary and ternary glass systems, J. Non-Crystal. Sol. 37 (1980) 359–365.
[18] N. Soga, Elastic moduli and fracture toughness of glass, J. Non-Crystal. Sol. 73 (1985) 3059–3313.
[19] G. Patriarche, E. Le Bourhis, D. Faurie, P.O. Renault, TEM study of the indentation behaviour of thin Au film on GaAs, Thin Solid Films 460 (2004) 150–155.
[20] J. Mencik, D. Munz, E. Quandt, E.R. Weppelmann, M.V. Swain, Determination of elastic modulus of thin layers using nanoindentation, J. Mater. Res. 12 (1997) 2475–2484.
[21] A. Perriot, E. Barthel, Elastic contact to a coated half-space: Effective elastic modulus and real penetration, J. Mater. Res. 19 (2004) 600.
[22] S. Bec, A. Tonck, J.L. Loubet, A simple guide to determine elastic properties of films on substrate from nanoindentation experiments, Phil. Mag. 86 (2006) 5347.
[23] H. Li, J.J. Vlassak, Determining the elastic modulus and hardness of an ultra-thin film on a substrate using nanoindentation, J. Mater. Res. 24 (2009) 1114.
[24] A. Tricoteaux, G. Duarte, D. Chicot, E. Le Bourhis, E. Bemporad, J. Lesage, Depth-sensing indentation modeling for determination of elastic modulus of thin films, Mech. of Mater. 42 (2010) 166.
[25] D. Beegan, M.T. Laugier, Application of composite hardness models to copper thin film hardness measurement, Surf. Coat. Technol. 199 (2005) 32.
[26] A.K. Bhattacharya, W.D. Nix, Analysis of elastic and plastic deformation associated with indentation testing of thin films on substrates, Int. J. Solids Struct. 24 (1988) 1287–1298.
[27] F. Mammeri, E. Le Bourhis, L. Rozes, C. Sanchez, A. Huignard, D. Lefevre, Time dependence of the indentation behavior of hybrid coatings, J. Non-Cryst. Sol. 345–346 (2004) 610–614.
[28] F. Mammeri, E. Le Bourhis, L. Rozes, C. Sanchez, Elaboration and mechanical characterization of nanocomposites thin films: Part I: Determination of the mechanical properties of thin films prepared by in situ polymerisation of tetraethoxysilane in poly(methyl methacrylate), J. Eur. Cer. Soc. 26 (2006) 259–266.
[29] G. Geandier, P.-O. Renault, E. Le Bourhis, Ph. Goudeau, D. Faurie, C. Le Bourlot, Ph. Djémia, O. Castelnau, S.M. Chérif, Elastic-strain distribution in metallic film–polymer substrate composites, Appl. Phys. Lett. 96 (2010) 041905.
[30] N. Chemin, L. Rozes, C. Chanéac, S. Cassaignon, E. Le Bourhis, J.-P. Jolivet, O. Spalla, E. Barthel, C. Sanchez, Structure and mechanical properties of mesostructured functional hybrid coatings based on anisotropic nanoparticles dispersed on poly(hydroxylethyl methacrylate), Chem. Mater. 20 (2008) 4602–4611.